Annals of Physics **283**, 308–333 (2000)
doi:10.1006/aphy.2000.6060, available online at http://www.idealibrary.com on IDEAL®

Single-Particle Self-Energy in Many-Body Systems at Finite Temperature

N. Giovanardi

Dipartimento di Fisica, Università di Milano, and INFN, Sezione di Milano, via Celoria 16, I-20133 Milano, Italy

P. Donati

Dipartimento di Fisica, Università di Milano, and INFN, Sezione di Milano, via Celoria 16, I-20133 Milano, Italy;
and The Niels Bohr Institute, University of Copenhagen, Copenhagen, Denmark

P. F. Bortignon

Dipartimento di Fisica, Università di Milano, and INFN, Sezione di Milano, via Celoria 16, I-20133 Milano, Italy

and

R. A. Broglia

Dipartimento di Fisica, Università di Milano, and INFN, Sezione di Milano, via Celoria 16, I-20133 Milano, Italy;
and The Niels Bohr Institute, University of Copenhagen, Copenhagen, Denmark
E-mail: ricardo.broglia@mi.infn.it

Received June 1, 1998; revised February 9, 2000

The properties of the self-energy of single-particle states in different many-body systems are studied as a function of the excitation energy ω and of the temperature T of the system. Two cases are considered: the coupling to uncorrelated and to correlated particle-hole excitations. © 2000 Academic Press

1. INTRODUCTION

Mean field is one of the most useful approximations in all of physics and chemistry. In it one replaces the many-particle Schrödinger equation by a single-particle Schrödinger equation. The many-body effects come in via the single-particle potential which is generated from the particles themselves. This potential not only confines the motion of the particles, but also renormalizes the single-particle properties in processes where particles, bouncing inelastically off the surface of the

0003-4916/00 $35.00

system set it into a vibration, vibrations which are eventually reabsorbed at a later stage by the same particle. These processes can also be generated by particle-particle collisions. The relative importance of these mechanisms through which particle-hole modes are excited varies from system to system, depending on impurities, geometry, densities, etc. The interweaving of single-particle motion and of vibrational modes gives rise to dressed particles, quasiparticles, displaying effective masses and charges, as well as finite lifetimes. In other words, both the single-particle lifetime as well as the effective mass are determined by the single-particle self-energy, an additional amount of energy the particle acquires as a consequence of its coupling to collective and non-collective modes of excitation of the system. This "extra" energy is proportional to the strength with which the particle couples to these modes, while its dependence on energy (ω) and temperature (T) is determined by the momentum content of the particle-vibration coupling vertex and by the frequency and temperature dependence of the response function associated with these excitations. Consequently, in systems like the atomic nucleus or small metal clusters [1], where the dynamical behaviour of the surface collects in a single or in few modes the full strength of particle-hole excitations, the renormalization of the single-particle properties is to be ascribed to the coupling of particles to collective vibrations of the surface. The coupling to uncorrelated particle-hole excitations leads, in this case, to small renormalization effects, as it proceeds through non-collective modes which have essentially given all their strength to low-lying collective vibrations or to high-lying giant resonances [2].

In the present paper we discuss, making use of the unifying formalism of thermal Green's functions developed by Matsubara [3], the consequences of the dressing of single-particles in infinite, semi-infinite, and finite systems, paying special attention to the frequency and temperature dependence of the associated (effective) observables.

While much is known concerning these quantities in the case of both finite and infinite systems (cf., e.g., [1–5] and references therein), the corresponding results have not been previously discussed as particular examples, or limiting situations, of a unified picture of many-body systems, nor have they been analyzed in terms of analytic or quasi-analytic solutions of realistic models. In particular, while in Refs. [6–8] the temperature behaviour of the effective mass in finite nuclei was calculated, no in depth discussion of the observed behaviour was carried out, while in the present paper we evidence, even analytically, the physics and the mathematics which are at the basis of this behaviour and compare it to what is known concerning these phenomena for the case of infinite systems.

The systematic development of the slab model [9] both at zero and at finite temperature has been instrumental in working out such a picture, in keeping with the fact that the slab model displays, on almost equal footing, properties of both finite and infinite systems. The systematic discussion of the corresponding results is carried out below.

In all the examples discussed, particles are assumed to interact through a two-body separable residual interaction (without exchange terms) of the form

$$v(r, r') = kF(r)\, F(r'), \tag{1}$$

where the coupling constant k and the single-particle fields F will be specified in each case. This approximation simplifies considerably the discussion without implying any significant loss of generality, as has been checked by comparing the separable force results with the results of so-called realistic interactions (cf., e.g, [10, 11]).

In Section 2 we discuss the coupling of single-particle motion to uncorrelated particle-hole excitations in infinite systems, while Section 3 deals with the renormalization effects associated with the coupling of single-particle motion to vibrations of the surface of a semi-infinite system (slab model). In Section 4 the insight obtained on the behaviour of the single-particle self-energy as a function of ω and T is used to discuss results obtained for the case of finite nuclei [6–8]. In particular, the temperature dependence of the effective mass published previously [6] is here shown to arise from a combined effect of universal phase space behaviour and of individual behaviour of low-lying collective surface vibrations. Section 5 contains the conclusions of the present work. A number of appendices are provided, where the explicit finite temperature expressions of building blocks (response functions of collective and non-collective particle-hole excitations and the corresponding self-energies, associated with the coupling of these modes to single-particle motion) of the physical quantities characterizing the quasiparticles (effective mass and lifetime) are collected.

2. THE SINGLE-PARTICLE SELF-ENERGY FROM THE COUPLING TO UNCORRELATED PARTICLE-HOLE STATES

In this section, we study the role collisions between particles and uncorrelated particle-hole excitations, as depicted by the diagram shown in Fig. 1a, have on the properties of the system. For the present discussion, the detailed form of the coupling constant k and of the field F of Eq. (1) is not important. In any case, we assume $F(r)$ to be dimensionless and k to have energy dimensions.

We first introduce the finite temperature unperturbed response function (cf. Appendix A),

$$R^0(\varepsilon, T) = \sum_{nm} F_{nm}^2 n_F(m) \left(\frac{1}{\varepsilon - \varepsilon_n + \varepsilon_m + i\eta} - \frac{1}{\varepsilon + \varepsilon_n - \varepsilon_m + i\eta} \right), \tag{2}$$

and the single-particle self-energy contribution associated to the graph in Fig. 1a (cf. Appendix B)

$$\Sigma_i^{ret}(\varepsilon, T) = -k^2 \sum_f F_{if}^2 \sum_{nm} F_{nm}^2 n_F(m) \left[\frac{1 + n_B(\varepsilon_{nm}) - n_F(\varepsilon_f)}{\varepsilon + i\eta - (\varepsilon_f + \varepsilon_{nm})} - \{\varepsilon_{nm} \to -\varepsilon_{nm}\} \right]. \tag{3}$$

In the above expressions, F_{if} is the matrix element of the field F between the single-particle states i and f, $\varepsilon_{nm} = \varepsilon_n - \varepsilon_m$, and n_F and n_B are Fermi and Bose occupation factors, respectively. The sums run over the energy eigenstates of the system, the

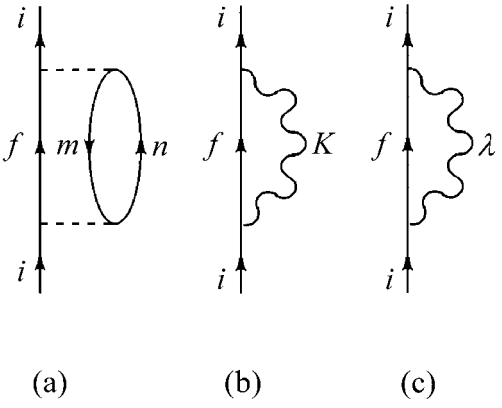

FIG. 1. Lowest order self-energy process due to the coupling of the single-particle state i to (a) an uncorrelated particle-hole, (b) a surface vibration whose wavenumber is K, and (c) a surface vibration of multipolarity λ.

single-particle energies ε_k being measured from the Fermi energy. They are kept temperature independent as expected for T values much smaller than ε_F. The imaginary part of Eq. (3), in the limit $\eta \to 0$, leads to

$$\text{Im } \Sigma_i^{ret}(\varepsilon, T) = -k^2 \sum_f F_{if}^2 (1 + n_B(\varepsilon - \varepsilon_f) - n_F(\varepsilon_f)) \text{ Im } R^0(\varepsilon - \varepsilon_f, T). \tag{4}$$

When dealing with infinite systems, and thus with continuum spectra, the sum over the states is replaced by an integral over the energy weighted by the level density of the system $g(\varepsilon)$. Using the mean value $\bar{F}_{if}$ of the single-particle matrix elements F_{if}, Eq. (4) becomes

$$\text{Im } \Sigma_i^{ret}(\varepsilon, T) = -k^2 \bar{F}_{if}^2 \int_{-\infty}^{+\infty} d\omega \; g(\omega)(n_B(\omega) + n_F(\omega - \varepsilon)) \text{ Im } R^0(\omega, T). \tag{5}$$

Throughout the paper, ε and ω are both energy variables.

As shown in Appendix A, Im $R^0(\omega, T)$ is, at long wavelengths, independent of T and linear in ω. For values of ε close to the Fermi energy, the occupation factors decay exponentially with ω. This behaviour suppresses the high-$|\omega|$ contribution to the integral in Eq. (5) and justifies the use of the (low-energy) linear approximation for Im $R^0(\omega, T)$, as well as the assumption of a constant level density g_0. One thus obtains (cf. Appendix B)

$$\begin{aligned} \text{Im } \Sigma_i^{ret}(\varepsilon, T) &= 2\pi \bar{v}^2 g_0^3 \int_{-\infty}^{+\infty} d\omega (n_B(\omega) + n_F(\omega - \varepsilon)) \, \omega \\ &= \pi \bar{v}^2 g_0^3 [(\pi T)^2 + \varepsilon^2], \end{aligned} \tag{6}$$

with $\bar{v} = k\bar{F}_{nm}\bar{F}_{if}$. Therefore Eq. (6) is an approximation of Im Σ holding around the Fermi energy. This is the region where temperature modifies the state of motion of the particles and where the most conspicuous temperature dependence of Im Σ is found.

Because the single-particle damping width $\Gamma_p^{\downarrow}$ is related to Im Σ [12], we conclude that the single-particle damping width increases quadratically with the temperature of the system. This result was obtained for the first time by Morél and Nozières [13] in the study of the lifetime of quasiparticles in ^{3}He.

The real part of the single-particle self-energy may be obtained from the imaginary part Im $\Sigma_i^{ret}(\varepsilon, T)$, by means of the Kramers–Krönig dispersion relation [11],

$$\text{Re } \Sigma_i^{ret}(\varepsilon, T) = \frac{1}{\pi} \mathscr{P} \int_{-\infty}^{+\infty} d\varepsilon' \frac{\text{Im } \Sigma_i^{ret}(\varepsilon', T)}{\varepsilon - \varepsilon'}, \tag{7}$$

where $\mathscr{P}$ stands for principal value of the integral. The temperature dependence of Re $\Sigma_i^{ret}(\varepsilon, T)$ is determined by the temperature dependence of Im $\Sigma_i^{ret}(\varepsilon, T)$. Therefore it is possible to find a value c such that Eq. (6) is valid for $|\varepsilon| < c$, and, as a consequence, write

$$\text{Re } \Sigma_i^{ret}(\varepsilon, T) \approx \frac{1}{\pi} \mathscr{P} \int_{-c}^{+c} d\varepsilon' \frac{\text{Im } \Sigma_i^{ret}(\varepsilon', T)}{\varepsilon - \varepsilon'} + f(\varepsilon), \tag{8}$$

where f is essentially independent of T (for a discussion about the convergence conditions of f, see Ref. [11]).

The average properties of Re Σ may be expressed in terms of the effective single-particle ω-mass [11],

$$m_\omega = m + \Delta m_\omega, \tag{9}$$

where

$$\Delta m_\omega = -m \left(\frac{d \text{ Re } \Sigma^{ret}(\varepsilon, T)}{d\varepsilon} \right)_{\varepsilon = 0}. \tag{10}$$

The temperature dependence of the effective mass is then controlled by the first integral in Eq. (8), that is,

$$\bar{v}^2 g_0^3 \mathscr{P} \int_{-c}^{+c} d\varepsilon' \frac{(\pi T)^2 + \varepsilon'^2}{\varepsilon - \varepsilon'} = -\bar{v}^2 g_0^3 \left[2\varepsilon c + (\varepsilon^2 + (\pi T)^2) \ln \left(\frac{c - \varepsilon}{c + \varepsilon} \right) \right]. \tag{11}$$

The dependence of the ω-mass on temperature is then given by (see Appendix B)

$$\frac{\Delta m_\omega(T)}{m} \sim 2\bar{v}^2 g_0^3 c \left[1 - \left(\frac{\pi T}{c} \right)^2 \right]. \tag{12}$$

The ω-mass is obtained by adding to this term the contribution arising from the temperature-independent parts of Re Σ.

The decrease of the ω-mass with temperature is thus a phase-space effect, reflecting, as pointed out in Ref. [14], the fact that the Fermi occupation factors $n_F(\varepsilon_f)$ of the intermediate single-particle states f (cf. Fig. 1a) approach the value $\frac{1}{2}$ at very high temperatures. In this limit, Eq. (3) becomes

$$\Sigma_i^{ret}(\varepsilon, T) \to -\frac{1}{2} \sum_{nm} F_{nm}^2 \left(\frac{1}{2} + n_B(\varepsilon_{nm}) \right) \times \sum_f F_{if}^2(\lambda) \left[\frac{1}{\varepsilon + i\eta - \varepsilon_f - \varepsilon_{nm}} + \{\varepsilon_{nm} \to -\varepsilon_{nm}\} \right]. \tag{13}$$

The real part of the sum over f then becomes a principal value integration of an odd function and then Re Σ vanishes.

3. SINGLE-PARTICLE SELF-ENERGY ARISING FROM THE COUPLING TO THE SURFACE

In this section, we consider a system characterized by a highly dynamic surface, displaying collective states. To parallel the discussion carried out in Section 2, in connection with the coupling of single-particle states to non-collective particle-hole excitations, we simplify the problem referring to a semi-infinite Fermi liquid (Slab model [9]), where the particles are confined in the half-space $z < 0$ by a potential barrier having a Woods–Saxon form,

$$V(z) = V_0(1 + e^{-z/a_d})^{-1}. \tag{14}$$

Connection with the physics of the atomic nucleus is obtained choosing $V_0 =$ 45 MeV and $a_d = 0.75$ fm. Single-particle wavefunctions are plane waves in the direction parallel to the surface ((x, y)-plane), while, in the z-direction, are the solutions of the single-particle Hamiltonian

$$H_0 = \frac{-\hbar^2}{2m} \frac{d^2}{dz^2} + V(z). \tag{15}$$

Following Ref. [9], particles are assumed to interact through a separable interaction along the z axis of strength k_0 and single-particle form factors peaked at the surface, and through a Yukawa interaction of range a_r in a plane perpendicular to the z-axis, namely

$$v(\mathbf{r}, \mathbf{r}') = k_0\, g(|\mathbf{r}_p - \mathbf{r}'_p|)\; V'(z)\; V'(z'), \tag{16}$$

where $\mathbf{r}_p$ and $\mathbf{r}'_p$ are two vectors perpendicular to the z-axis and $V'(z)$ is the derivative of the potential defined in Eq. (14), while

$$g(r) = \frac{e^{r/a_r}}{2\pi a_r r}. \tag{17}$$

The value of the strength k_0 is determined by the equation [15]

$$k_0^{-1} = \int dz\, \rho'_0(z)\, V'(z), \tag{18}$$

which expresses the self-consistent relation existing between density and potential variations associated with normal modes. In keeping with translational invariance of the system along the (x, y)-plane, it is convenient to express the function given in Eq. (17), in terms of its two-dimensional Fourier transform, that is,

$$g(|\mathbf{r}_p - \mathbf{r}'_p|) = \int \frac{d^2\mathbf{K}}{(2\pi)^2}\, e^{i\mathbf{K}(\mathbf{r}_p - \mathbf{r}'_p)} \gamma(K), \tag{19}$$

$$\gamma(K) = \frac{1}{\sqrt{1 + (a_r K)^2}}. \tag{20}$$

The function $\gamma(K)$ is independent of the orientation of the momentum K, because of the invariance of the system with respect to rotations around z. Through Eq. (19), $v(\mathbf{r}, \mathbf{r}')$ can be written as a momentum integral of a completely separable interaction, of the same type of that given in Eq. (1),

$$v(\mathbf{r}, \mathbf{r}') = \int \frac{d^2\mathbf{K}}{(2\pi)^2}\, k_0 \gamma(K)\, F(\mathbf{K}, \mathbf{r})\, F^*(\mathbf{K}, \mathbf{r}'), \tag{21}$$

where the single-particle field is now

$$F(\mathbf{K}, \mathbf{r}) = e^{i\mathbf{K}\cdot\mathbf{r}_p} V'(z). \tag{22}$$

A connection between K in this model and the multipolarity λ of the surface vibrations in a finite system can be obtained via the asymptotic expansion for the Legendre polynomials [9],

$$P_\lambda(\cos\theta) \approx J_0(\lambda\theta) = J_0(K\rho), \tag{23}$$

where J_0 is a Bessel function while ρ measures the length of an arc over a sphere of radius R, and

$$K = \frac{\lambda}{R}. \tag{24}$$

$$F(\omega) = \int \frac{dK}{2\pi} K \ \mathrm{Im}\ R(K, \omega)$$

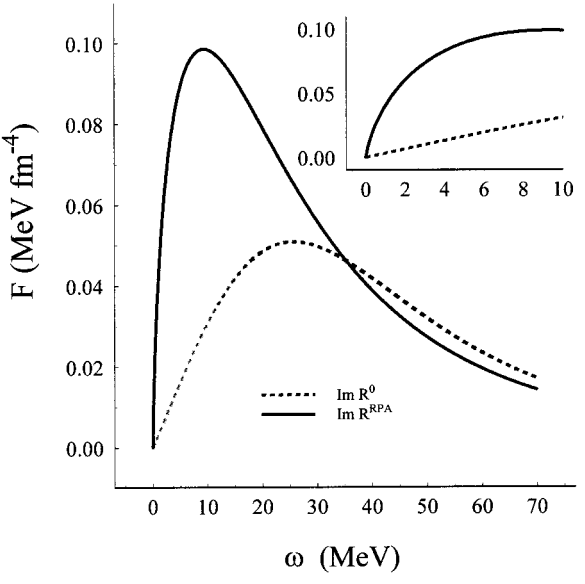

FIG. 2. The imaginary part of the unperturbed (dash) and RPA (solid) response functions in the slab model, integrated over the wavelength K. In the inset, the low-energy tail of the two integrated responses is shown.

Within the slab model, Im $R^0(\varepsilon, K)$ can be accurately parametrized in terms of the Lorentzian function (cf. [9, Eq. (3.1)])

$$\mathrm{Im}\ R^0(\varepsilon, K) = \frac{1}{\pi} N(K)\, \Gamma(K) \left(\frac{1}{(\varepsilon - E_0(K))^2 + \Gamma(K)^2} - \frac{1}{(\varepsilon + E_0(K))^2 + \Gamma(K)^2} \right). \tag{25}$$

The centroid $E_0(K)$ and width $\Gamma(K)$ correspond to the quantity $\hbar\omega_0(K)$ and $\hbar\gamma(K)/2$, defined in [9, Eq. (3.3)], where also the normalization $N(K)$ is defined. The integral of Im $R^0(\varepsilon, K)$ over d^2K is plotted in Fig. 2 (dashed line) and can be parametrized, for long wavelengths, as

$$\int \frac{d^2\mathbf{K}}{(2\pi)^2} \mathrm{Im}\ R^0(K, \omega) \approx \mathrm{const} \cdot \omega, \tag{26}$$

thus displaying the same linear behaviour with ω of the unperturbed response function discussed in the previous section (cf. Eq. (64)). The single-particle self-energy associated with the process shown in Fig. 1a is

$$\begin{aligned}\text{Im } \Sigma_i^{(0),\,ret}(\varepsilon, T) = & -k_0^2 \sum_f \int \frac{d^2\mathbf{K}}{(2\pi)^2} \gamma^2(K)\, F_{if}^2(K) \\ & \times (1 + n_B(\varepsilon - \varepsilon_f) - n_F(\varepsilon_f))\, \text{Im } R^0(K, \varepsilon - \varepsilon_f), \end{aligned} \tag{27}$$

where $F_{if}(K)$ are the single-particle matrix elements of the field $F(\mathbf{K}, \mathbf{r})$. As in Eq. (4), the label f is assumed to run over the energy eigenstates of the system. Limiting the discussion to the case of zero-range interaction among nucleons moving along the slab surface ($a_r = 0$ in Eq. (20)), the coupling constant reduces to k_0, independent from K, because $\gamma(K) = 1$. A finite range of the Yukawa potential would imply a reduced importance of the short wavelength surface deformations in the dressing process, due to the factor $(1 + (a_r K)^2)^{-1}$. Using the mean value $\bar{F}_{if}$ of $F_{if}(K)$ and replacing the sum over f with an integral, Eq. (27) becomes

$$\begin{aligned}\text{Im } \Sigma_i^{(0),\,ret}(\varepsilon, T) = & -k_0^2 \bar{F}_{if}^2 g_0 \int_{-\infty}^{+\infty} d\omega (n_B(\omega) + n_F(\omega - \varepsilon)) \\ & \times \int \frac{d^2\mathbf{K}}{(2\pi)^2} \text{Im } R^0(K, \omega). \end{aligned} \tag{28}$$

Assuming the approximation given by Eq. (26), Eq. (28) becomes

$$\text{Im } \Sigma_i^{(0),\,ret}(\varepsilon, T) = -k_0^2 \bar{F}_{if}^2 g_0 \int d\omega (n_B(\omega) + n_F(\omega - \varepsilon))\, \omega, \tag{29}$$

and the same quadratic rule found in the case of infinite systems is thus recovered (cf. Eq. (6)).

However, the physics of the surface dynamics is now described by the random phase approximation (RPA) response function [9],

$$R^{RPA}(K, \omega) = \frac{R^0(K, \omega)}{1 - k_0 \gamma(K)\, R^0(K, \omega)}, \tag{30}$$

displaying, in particular, a softening of the density response.

The most important single-particle dressing process is represented in this system by the coupling of the particles to the RPA surface vibrations of Eq. (30). It is described, to lowest order perturbation theory, by the process depicted in Fig. 1b. The imaginary part of the retarded self-energy associated to the graph drawn in Fig. 1b is given by

$$\begin{aligned}\text{Im } \Sigma_i^{ret}(\varepsilon, T) = & -k_0^2 \sum_f \int \frac{d^2\mathbf{K}}{(2\pi)^2} \gamma^2(K)\, F_{if}^2(K) \\ & \times (1 + n_B(\varepsilon - \varepsilon_f) - n_F(\varepsilon_f))\, \text{Im } R^{RPA}(K, \varepsilon - \varepsilon_f). \end{aligned} \tag{31}$$

Taking the mean value $\bar{F}_{if}$ of the single-particle matrix elements F^K_{if} and replacing the sum over f with an integral over the energy, as in Section 2, Eq. (31) may be written as

$$\text{Im}\,\Sigma^{ret}_i(\varepsilon, T) = -k_0^2 \bar{F}^2_{if} g_0 \int_{-\infty}^{+\infty} d\omega (n_B(\omega) + n_F(\omega - \varepsilon)) \times \int \frac{d^2\mathbf{K}}{(2\pi)^2} \text{Im}\, R^{RPA}(K, \omega), \tag{32}$$

where g_0 is the level density around the Fermi energy. From Fig. 2, and comparing Eqs. (32) and (28), one can see that the difference between Im Σ and Im Σ^0 is fully determined by the low-energy behaviour of the corresponding integrated response functions of the slab (unperturbed and RPA). It can be seen, in particular in the inset of Fig. 2, that the RPA response dominates and therefore the renormalization process is to be ascribed to the coupling among particles and RPA surface vibrations.

The RPA response function calculated numerically as a function of the temperature (thermal RPA, see e.g., Ref. [16]) shows an extremely weak temperature dependence, being dominated by the coupling to the continuum. One can thus use the analytic $T = 0$ low-energy expression (cf. Refs. [17, 18])

$$R^{RPA}(K, \omega) = \frac{k_0^{-2}}{ia\omega - \sigma K^2}, \tag{33}$$

for the exact calculation of the integral in Eq. (32), in the case of small $|\varepsilon|$ values. This is because, as already discussed in Section 2, the high frequency tail of the response is suppressed by the exponentially decaying occupation factors. In Eq. (33), k_0 is the coupling constant defined in Eq. (18), $\sigma \approx 1$ MeV fm^{-2} represents the surface tension of the system while $a \approx 0.157$ fm^{-4} is the friction constant defined[1] in Ref. [17]. The imaginary part of the response,

$$\text{Im}\, R^{RPA}(K, \omega) = -k_0^{-2} \frac{a\omega}{(a\omega)^2 + (\sigma K^2)^2}, \tag{34}$$

is a regular odd function vanishing as $a\omega$ at $\omega = 0$, for finite values of the wavenumber K. For $K = 0$, it diverges at $\omega = 0$ as $(a\omega)^{-1}$. This divergence reflects the existence of a Goldstone mode occurring at infinite wavelength surface deformations, as a consequence of the infinite geometry of this system. In fact, a $K = 0$ deformation corresponds to a displacement of the surface, moving parallel to itself, which costs no energy. In performing the sum over the surface deformations, that is, integrating Eq. (34) over d^2K, one obtains an integrated response which is not

[1] We point out that a, as defined in Eq. (9) of Ref. [17], is obtained by the parametrization in Eq. (3) of the same reference, which is defined unless $\hbar^{-1}$ and therefore $a\omega$ in Eq. (33) is given in MeV fm^{-4}.

defined for $\omega = 0$ and jumps from the constant value $(8\sigma)^{-1}$ to $-(8\sigma)^{-1}$ with a discontinuity at $\omega = 0$,

$$\int_0^\infty \frac{K\,dK}{2\pi} \operatorname{Im} R^{RPA}(\omega, K) = -\frac{k_0^{-2}}{8\sigma} [\theta(\omega) - \theta(-\omega)]. \tag{35}$$

The strength of the vibrations is constant over the whole excitation spectrum and is inversely proportional to the surface tension σ. Although the $\omega = 0$ divergence of the $K = 0$ response disappears in the integrated response, vibrational modes of arbitrarily small energy can be excited. This produces a divergence in the integral in Eq. (32), due to the fact that the Bose factor $n_B(\omega)$ diverges as ω^{-1} at $\omega = 0$. The exclusion of the Goldstone mode from the excitation spectrum is necessary to avoid the divergence. In fact this exclusion regularizes the $\omega = 0$ behaviour of the integrated response, which goes to zero as ω, erasing the Bose factor divergence. This is obtained by integrating over the K-spectrum starting from an arbitrarily small, but non-zero, K_0 value,

$$\int_{K_0}^\infty \frac{K\,dK}{2\pi} \operatorname{Im} R^{RPA}(\omega, K) = -\frac{k_0^{-2}}{4\pi\sigma} \arctan\left(\frac{a\omega}{\sigma K_0^2}\right). \tag{36}$$

The linear approximation of the integrated response, at low energies, comes from the first term in the Taylor expansion of the arc tangent. The width of the region around $\omega = 0$ where the linear behaviour dominates is inversely proportional to K_0. Aiming at giving an analytical solution to the integral in Eq. (32), we approximate the integrated response with its asymptotic value for $|\omega| > \omega_0$, that is,

$$\int_0^\infty \frac{K\,dK}{2\pi} \operatorname{Im} R^{RPA}(\omega, K) \overset{|\omega| \geq \omega_0}{\approx} -\frac{K_0^2}{8\sigma} [\theta(\omega - \omega_0) - \theta(-\omega - \omega_0)], \tag{37}$$

and with

$$\int_{K_0}^\infty \frac{K\,dK}{2\pi} \operatorname{Im} \mathrm{R}^{RPA}(\omega, K) \overset{|\omega| \leq \omega_0}{\approx} -\frac{k_0^{-2} a\omega}{4\pi(\sigma K_0^2)} = -\frac{k_0^{-2}}{8\sigma} \frac{\omega}{\omega_0}, \tag{38}$$

for $|\omega| < \omega_0$, where $\omega_0 = \pi\sigma K_0^2/(2a)$. Choosing K_0 of the order of $0.1\ \mathrm{fm}^{-1}$, then $\omega_0(K_0) \approx 10 K_0^2\ \mathrm{MeV\ fm}^2 \approx 0.1\ \mathrm{MeV}$. The imaginary part of the self-energy can be then calculated,

$$\operatorname{Im} \Sigma_i^{ret}(\varepsilon, T) = -\frac{\bar{F}_{if}^2}{8\sigma} g_0 T \left(\ln[n_F(\varepsilon - \omega_0)(1 - n_F(\varepsilon + \omega_0))] - f\left(\frac{\omega_0}{T}\right)\right), \tag{39}$$

where

$$f\left(\frac{\omega_0}{T}\right) = 2[1 + \ln(1 + n_B(\omega_0))], \tag{40}$$

as shown in Appendix C. The validity of this expression is limited to energy values around the Fermi energy, for the same reasons discussed in the previous section, about Eq. (6). The energy dependence is contained in the first term of Eq. (39), through the Fermi occupation factors.

The behaviour of Im Σ at the Fermi energy ($\varepsilon = 0$) as a function of T is then

$$\text{Im } \Sigma_i^{ret}(\varepsilon = 0,\, T) = \frac{\bar{F}_{if}^2}{4\sigma}\, g_0 T \left[\ln \frac{1 + n_B(\omega_0)}{1 - n_F(\omega_0)} + 1 \right]. \tag{41}$$

This function has a quasi-linear slope. Consequently, the single particle damping width of a particle at the Fermi energy is expected to increase as a linear function of the temperature. More precisely, from Eq. (41) we find that

$$\text{Im } \Sigma_i^{ret}(\varepsilon = 0,\, T = 0) = 0, \tag{42}$$

while its high-T expansion gives

$$\text{Im } \Sigma_i^{ret}(\varepsilon = 0,\, T \gg \omega_0) = \frac{\bar{F}_{if}^2}{4\sigma}\, g_0 \left[T \left(1 - \ln \frac{\omega_0}{2} \right) + T \ln T \right]. \tag{43}$$

The condition $T \gg \omega_0$ is fulfilled over the most part of the temperature range of interest, ω_0 being of the order of 0.1 MeV. The behaviour of the imaginary part of the self-energy is then given as the sum of a linear term in T and a term growing faster than T, namely as $T \ln T$. The linear term in T has a large coefficient and dominates in the global behaviour.

At zero temperature, Eq. (39) becomes

$$\text{Im } \Sigma_i^{ret}(\varepsilon, 0) = \frac{\bar{F}_{if}^2}{8\sigma}\, g_0 [-(\varepsilon + \omega_0)(1 - \theta(\varepsilon + \omega_0)) + (\varepsilon - \omega_0)\, \theta(\varepsilon - \omega_0)]. \tag{44}$$

The exclusion of the Goldstone mode from the RPA response implies the suppression of Im Σ in the region $|\varepsilon| < \omega_0$. Indeed, if the RPA response below ω_0 is suppressed, a particle having an energy $|\varepsilon| < \omega_0$ does not couple to any vibrational state and has zero damping width.

The result of Ref. [18],

$$\text{Im } \Sigma_i^{ret}(\varepsilon, 0) = \frac{\bar{F}_{if}^2}{8\sigma}\, g_0\, |\varepsilon|, \tag{45}$$

is obtained in the limit $\omega_0 \to 0$ of Eq. (44). A finite value of ω_0 is not necessary, at zero temperature, because the Bose factor in the integral of Eq. (32) becomes zero and no divergence takes place.

An approximation of Eq. (39) is given by

$$\text{Im}\ \Sigma_i^{ret}(\varepsilon, T) \approx \frac{\bar{F}_{if}^2}{8\sigma} g_0 \left[\sqrt{\varepsilon^2 + (2 \ln 2T)^2} + Tf\left(\frac{\omega_0}{T}\right)\right], \tag{46}$$

where, in the ε-dependent part of Im Σ, ω_0 has been neglected, in keeping with the fact that it is of the order of 0.1 MeV.

In the calculation of the real part of the single-particle self-energy, we follow the same scheme used in the previous section, adopting the approximation introduced in Eq. (8). Moreover, in solving the principal value integral, it is convenient to use the approximated expression in Eq. (46), leading to

$$\frac{1}{\pi} \mathscr{P} \int_{-c}^{+c} d\varepsilon' \frac{\text{Im}\ \Sigma_i^{ret}(\varepsilon', T)}{\varepsilon - \varepsilon'} = -\frac{\bar{F}_{if}^2}{8\pi\sigma} g_0 \left[\sqrt{\varepsilon^2 + (\alpha T)^2} \ln \frac{|\varepsilon - c|\ f_-(\varepsilon, T, c)}{|\varepsilon + c|\ f_+(\varepsilon, T, c)} + \varepsilon \ln \frac{g_+(T, c)}{g_-(T, c)} + Tf\left(\frac{\omega_0}{T}\right) \ln \left|\frac{c - \varepsilon}{c + \varepsilon}\right| \right], \tag{47}$$

where $\alpha = 2 \ln 2$,

$$f_\pm(\varepsilon, T, c) = (\alpha T)^2 \pm \varepsilon c + \sqrt{(\varepsilon^2 + (\alpha T)^2)(c^2 + (\alpha T)^2)}, \tag{48}$$

and

$$g_\pm(T, c) = \sqrt{c^2 + (\alpha T)^2} \pm c. \tag{49}$$

From the derivative at the Fermi energy of Eq. (47), the variation of the ω-mass of a particle at the Fermi energy as a function of T can be written as

$$\frac{\Delta m_\omega(T)}{m} = -\frac{\bar{F}_{if}^2}{4\pi\sigma} g_0 \left[\frac{T}{c} \left(\alpha + f\left(\frac{\omega_0}{T}\right)\right) + \frac{c}{\alpha T + \sqrt{c^2 + (\alpha T)^2}} - \frac{1}{2} \ln \frac{g_+(T, c)}{g_-(T, c)} \right]. \tag{50}$$

Its behaviour is dominated by the logarithmic term $\ln g_-(T, c)$ and by the term $Tf(\omega_0/T)/c$. The other terms behave essentially as a constant over a wide range of temperatures. An accurate approximation of Eq. (50) is provided by

$$\frac{\Delta m_\omega(T)}{m} = -\frac{\bar{F}_{if}^2}{4\pi\sigma} g_0 (\ln T + k_1 T \ln T + k_2 T + k_3), \tag{51}$$

with the constants $k_1 = 2/c$, $k_2 = k_1(1 - \ln \omega_0)$ and $k_3 = 1 + \ln(\alpha/2c)$. The divergence in the zero temperature limit is due to the non-analyticity of Im $\Sigma(\varepsilon, 0)$ at $\varepsilon = 0$ (cf. Eqs. (44) and (46)). This result then displays the same logarithmic divergence found in Ref. [18], which is a feature of this particular system, where only continuum excitation spectra are involved. As already discussed in the case of the coupling to uncorrelated particle-hole excitations, the decreasing of the ω-mass is a consequence of the progressive opening, with the temperature, of the phase-space available to a particle at the Fermi energy.

4. THE CASE OF THE ATOMIC NUCLEUS

In the case of atomic nuclei, the nuclear surface plays a dominant role in the particle dynamics [2]. The surface vibrations are calculated in RPA, and the spectrum has a discrete part, as a rule, due to the finite geometry of the system. The most collective of the RPA modes are those to which a large number of particle-hole excitations contribute, in a coherent fashion. This can be seen from Fig. 3a, where the low-energy tail of the functions Im $R^{RPA}(\omega)$ and Im $R^0(\omega)$, for the nucleus ^{98}Mo, are displayed, at the temperature $T = 2$ MeV. Here the RPA has been obtained from the relation [15],

$$R_\lambda^{RPA}(\omega, T) = R_\lambda^0(\omega, T)(1 - k_\lambda R_\lambda^0(\omega, T))^{-1}. \tag{52}$$

We have used a separable residual interaction of the form given in Eq. (1), where the single-particle fields are given by

$$F(r, \theta, \phi) = -R_0 \frac{\partial V}{\partial r} Y_\lambda^*(\theta, \phi), \tag{53}$$

being R_0 the nuclear radius and $V(r)$ a Woods–Saxon potential with standard parameters. The coupling constants k_λ were determined by the self-consistent relation given in Eq. (18), where in this case z represents the radial coordinate r. The unperturbed response appears to be one order of magnitude lower than the RPA response. Moreover it can be observed that the last displays a rather well defined plateau (over which the peaks of the most collective 2^+ and 3^- states appear) with a rather constant excitation probability of the surface vibrations, and a rapid fall off to zero, in a sharp region around $\omega = 0$. An arc tangent function is superimposed (in arbitrary units), to compare the RPA response in molibdenum and the low-energy tail of the RPA response in the slab model (cf. Eq. (36)). The unperturbed response is also plotted in Fig. 3b, in an expanded scale, for a comparison with the linear increasing predicted in the case of a continuous spectrum. In Fig. 3c, the temperature dependence of the total RPA response in ^{120}Sn (the sum of the $\lambda = 2$, 3, 4, and 5 contributions) is pointed out.

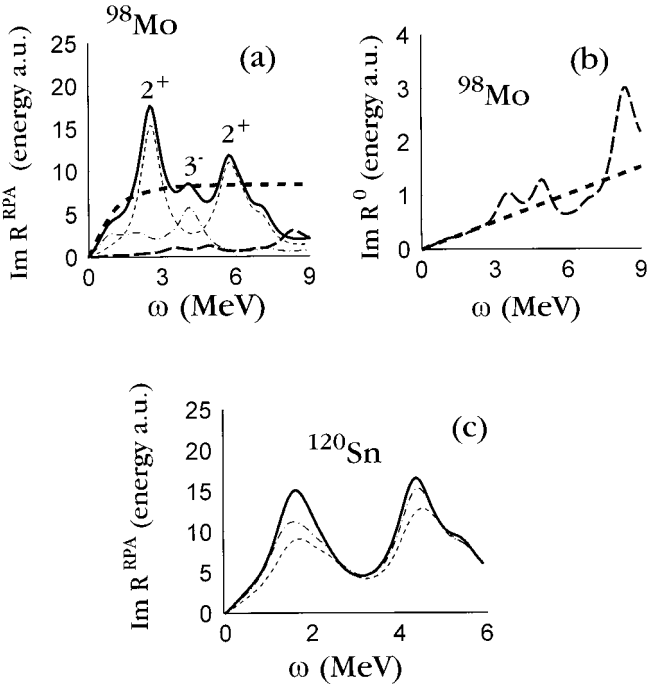

FIG. 3. (a) The low-energy tail of the imaginary part of the RPA response of ^{98}Mo is shown. We plot the curves in arbitrary energy units, which are independent from the multipolarity. The dashed and dash-dotted curves are related to the quadrupole and octupole responses, while the thick solid curve corresponds to their sum. The RPA calculations have been performed at $T = 2$ MeV. The thick short-dashed curve represents an arc tangent function which (in arbitrary units) is the behaviour of the RPA response in the slab model. The thick long-dashed curve, on the bottom of the graph, is the unperturbed response of ^{98}Mo. In (b) the unperturbed response of ^{98}Mo is shown in an expanded scale, superposed to a straight line, representing the analytical behaviour of Im R^0. This response essentially does not change with temperature. In (c) the total RPA response in ^{120}Sn (the sum of the $\lambda = 2$, 3, 4, and 5 contributions) is shown. The solid, dash-dotted, and dotted lines correspond to the temperatures $T = 0.5$, 1, and 2 MeV, respectively. All the response functions shown here have been calculated with an averaging parameter $\eta = 0.5$ MeV.

The single-particle self-energy (graph of Fig. 1c) is now written as [20]

$$\Sigma_i^{ret}(\varepsilon, T) = -\sum_{\lambda} \sum_{f} F_{if}^2(\lambda) \sum_{n(\lambda)} \beta_n^2 \left[\frac{1 + n_B(\omega_n) - n_F(\varepsilon_f)}{\varepsilon + i\eta - (\varepsilon_f + \omega_n)} - \{\omega_n \to -\omega_n\} \right], \qquad (54)$$

where λ is the multipolarity of the surface vibration and with the typical values of the averaging parameter $\eta \approx 0.5$ MeV, which approximately takes into account the coupling to more complex states than the doorways here considered [19] in the hierarchy of the intermediate states [21]. It is noted that, for both graphs in Figs. 1b and 1c, the Pauli principle violating contributions are expected to be small,

for coupling to very collective states, and may be corrected for including higher order terms (see [20]).

From the real and imaginary parts of the single-particle self-energy, the single-particle strength-function is written as [12]

$$S_i(\varepsilon, T) = \frac{1}{\pi} \frac{\text{Im } \Sigma_i(\varepsilon, T) + \eta}{(\varepsilon_i + \text{Re } \Sigma_i(\varepsilon, T) - \varepsilon)^2 + (\text{Im } \Sigma_i(\varepsilon, T) + \eta)^2}. \tag{55}$$

It represents the energy distribution probability of the single-particle state i.

The single-particle self-energy has been calculated in Refs. [6–8, 14, 20] for a number of single-particle states lying around the Fermi energy, in a range of temperatures $T = 0$–3 MeV, and in different nuclei, ^{208}Pb, ^{120}Sn, ^{98}Mo, and ^{64}Zn. For each temperature, an average value of the self-energy has been defined

$$\bar{\Sigma}(\varepsilon, T) = \frac{\sum_n (2j_n + 1)\, \Sigma_{j_n}(\varepsilon, T)}{\sum_n (2j_n + 1)}, \tag{56}$$

where the sum runs over a number of states and the factor $(2j_n + 1)$ has been introduced in order to take into account the degeneracy of each of these states. As a result, an approximatively linear increasing of Im $\bar{\Sigma}(\varepsilon, T)$ with the temperature has been found, confirming the predictions of the slab model; see Fig. 4 and Eq. (46). From the real and imaginary part of Σ, all the related strength functions have been obtained and the single-particle spreading widths $\Gamma_p^{\downarrow}$ extracted as the full width at half maximum (FWHM). This has been done because, although the imaginary part of the self-energy is often identified with the width of the state, the energy dependence of the real part, which appears in the energy denominator of Eq. (52), affects the FWHM in a non-trivial way. This is the reason why Im Σ cannot be identified with the width, but simply assumed to represent its most important contribution. It is found that the linear increase of Im Σ with T reflects in an approximate linear increase of $\Gamma_p^{\downarrow}(T)$ (see Fig. 5). In Fig. 5a, the FWHM is displayed also for states at about 8 MeV from the Fermi level, playing a major role in the physics of the giant resonances. It is observed that the increase with T of $\Gamma_p^{\downarrow}(T)$ is much weaker than for states at the Fermi energy [8], in keeping with the fact that the thermal smoothing of the Fermi surface affects mainly states close to it. Zero-temperature values are in overall agreement with the available experimental data [22].

Also in the case of finite nuclei the real part of the self-energy is found to flatten, at the Fermi energy, when the temperature of the nucleus increases, and so the ω-mass is found to be a decreasing function of the temperature. It can be parametrized according to [6]

$$\Delta m_\omega(T) = \Delta m_\omega(0)\, e^{-T/T_0}, \tag{57}$$

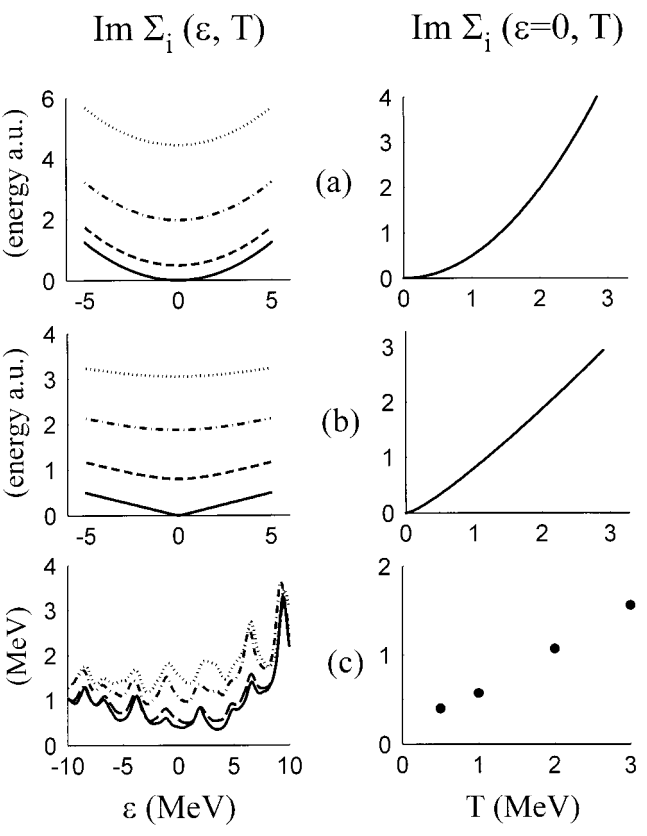

FIG. 4. Imaginary part of the self-energy of a single-particle state, due to the coupling to (a) uncorrelated particle-hole excitations in an infinite or semi-infinite system, corresponding to the graphical representation of Eq. (6), for $T=0$, 1, 2, and 3 MeV (solid, dash, dash-dot, and dot lines, respectively); (b) to surface vibrations in the Slab Model, corresponding to the graphical representation of Eq. (39), for $\omega_0=0.1$ MeV and for $T=0$, 1, 2, and 3 MeV (same convention of (a) for the lines). In (c) the same function is shown [8] for an average of single-particle states around the Fermi energy in the nucleus ^{120}Sn at $T=0.5$, 1, 2, and 3 MeV (solid, dash, dash-dot, and dot lines, respectively), where the averaging parameter $\eta=0.5$ MeV has been used. On the right of each graph, the corresponding behaviour of Im $\Sigma(\varepsilon=0, T)$ is reported. In both (a) and (b) figures, arbitrary units are used for the plotted functions. In (c), Im Σ is given in MeV.

where $T_0 \approx 1/5-2$ MeV, and depends on the nucleus considered, reflecting the energy of the low-lying collective modes. In this case, the ω-mass decreasing is not only a consequence of phase space effects, as discussed in the previous sections, but also of the collectivity loss of these low-lying modes (see Fig. 3c). The increase $\Delta m_\omega(0)$ can be as large as 0.5 [6, 11], consistent with the empirical evidence [2, 11], whereas the temperature dependence is in qualitative agreement with the behaviour of the level density parameter a, proportional to the effective mass [2].

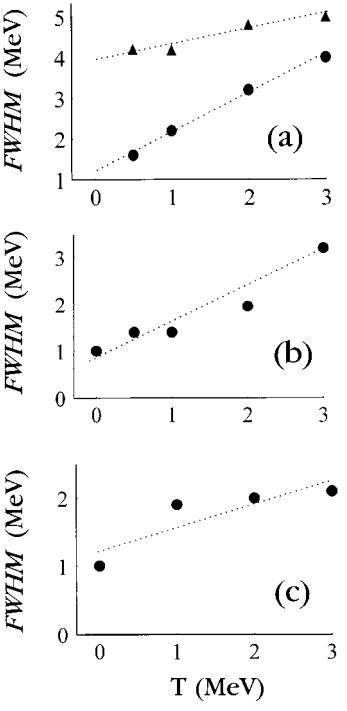

FIG. 5. The behaviour of $\Gamma^{\downarrow}_{s.p.}$ (measured as the full width at half maximum of the single-particle strength functions) in (a) ^{120}Sn [8], in (b) ^{98}Mo [7] and in (c) ^{64}Zn [7] as a function of the temperature, calculated from an average of single-particle states around the Fermi energy. In (a) also $\Gamma^{\downarrow}_{s.p.}$ for an average of states around 8 MeV far from the Fermi surface is displayed (triangles). An averaging parameter $\eta = 0.5$ MeV has been used. States at the Fermi energy have a finite width also at zero temperature, because of a finite averaging parameter and of a finite pairing gap, leading to a non-vanishing imaginary part of the self-energy.

The numerical results of the calculation of the effective mass in the case of ^{98}Mo and ^{64}Zn are displayed in Fig. 6 and are compared to the analytical results obtained in the case of coupling to uncorrelated p-h states, Eq. (12), and to surface vibrations of the slab model, Eq. (51). The corresponding curves have been obtained rescaling the analytical formulas with an arbitrary factor. In the case of coupling to surface vibrations, four curves have been plotted for different values of the cutoff c in the Kramers–Krönig integral, and a value $\omega_0 = 1.5$ MeV has been set, of the order of the lowest RPA roots energy. However, it must be pointed out that, besides the different behaviour of Δm_ω versus temperature, the contribution to the effective mass due to the coupling to surface vibrations is about an order of magnitude larger than the contribution due to the coupling to unperturbed particle-holes, because of the difference among the self-energies in the two cases.

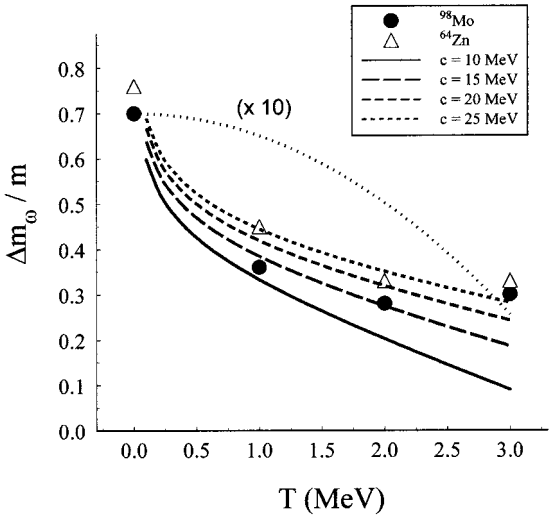

FIG. 6. Decreasing of $\Delta m_\omega(T)/m$ as a function of the temperature in the case of coupling of nucleons at the Fermi energy to surface vibrations in finite nuclei [6]. Empty triangles are related to the nucleus ^{98}Mo and full spots to ^{64}Zn. The superposed curves represent the analytical behaviour in the case of coupling to uncorrelated particle-holes (dots) and to surface vibrations at different values of the cutoff c. These curves have been rescaled with an arbitrary factor in order to have the same magnitude of the numerical results.

5. CONCLUSIONS

The single-particle self-energy has been calculated within the framework of thermal Green's functions (Matsubara), paying special attention to the associated damping width $\Gamma_p^\downarrow$ and the effective mass. Depending on which kind of coupling dominates in the particle "dressing" process, the behaviour of $\Gamma_p^\downarrow$ as a function of temperature T is quite different. This difference is to be ascribed to the different behaviour of the response function of uncorrelated particle-hole excitations and surface vibrations. In fact, the imaginary part of the single-particle self-energy, giving the particle a finite lifetime and, as a consequence, a damping width, has the same structure in both cases,

$$\text{Im}\,\Sigma_i^{ret}(\varepsilon, T) = -\sum_f F_{if}^2(1 + n_B(\varepsilon - \varepsilon_f) - n_F(\varepsilon_f))\,\text{Im}\,R(\varepsilon - \varepsilon_f), \tag{58}$$

where Im $R(\varepsilon)$ is the imaginary part of the response function of the state (particle-hole or surface vibration) the particle couples to. The coupling with uncorrelated particle-hole (but, at finite temperature, also particle-particle and hole-hole) excitations leads to a quadratic dependence while, in the case of the coupling to collective modes, the dependence is essentially linear. We have found that in both cases the real part of the self-energy flattens out around the Fermi energy, as the temperature

increases, implying that the effective mass (ω-mass) decreases as the system is heated.

APPENDIX A

In this appendix a general expression of the unperturbed response function $R^0(\varepsilon, T)$ of a finite temperature many-body system to an external field $\hat{F}$ and its low-energy approximation, in the case of infinite systems, are given.

The response function $R^0(\varepsilon, T)$ to the field $\hat{F}$ is obtained as the sum over n and m of the so-called "bubble" diagrams

$$\frac{1}{\beta}\sum_{\nu=-\infty}^{+\infty} \mathcal{G}^0(m, ip'_\nu)\,\mathcal{G}^0(n, ip'_\nu + ip_\nu) = \frac{n_F(\varepsilon_m) - n_F(\varepsilon_n)}{ip_\nu - \varepsilon_n + \varepsilon_m}, \tag{59}$$

weighted by the corresponding square matrix elements of the external field between the unperturbed single-particle states, $F^2_{nm} = |\langle n|\,\hat{F}\,|m\rangle|^2$. In Eq. (59), the fermionic Green's function

$$\mathcal{G}^0(j, ip_\nu) = \frac{1}{ip_\nu - \varepsilon_j}, \tag{60}$$

is defined, ε_j being the energy of the single-particle state j (measured with respect to the Fermi energy), n_F the Fermi occupation factor, and p_ν the odd discrete frequency

$$p_\nu = \frac{(2\nu+1)\,\pi}{\beta}. \tag{61}$$

After the substitution $ip_\nu \to \varepsilon + i\eta$ in Eq. (59), where η is a positive and arbitrarily small parameter, the following expression is found,

$$\begin{aligned} R^0(\varepsilon, T) &= \sum_{nm} F^2_{nm}\,\frac{n_F(\varepsilon_m) - n_F(\varepsilon_n)}{\varepsilon + i\eta - \varepsilon_n + \varepsilon_m} \\ &= \sum_{nm} F^2_{nm} n_F(\varepsilon_m)\left[\frac{1}{\varepsilon + i\eta - \varepsilon_n + \varepsilon_m} - \frac{1}{\varepsilon + i\eta + \varepsilon_n - \varepsilon_m}\right]. \end{aligned} \tag{62}$$

Its imaginary part, in the $\eta \to 0$ limit, is given by

$$\mathrm{Im}\, R^0(\varepsilon, T) = -\pi \sum_{nm} F^2_{nm} n_F(m)(\delta(\varepsilon - \varepsilon_n + \varepsilon_m) - \delta(\varepsilon + \varepsilon_n - \varepsilon_m)). \tag{63}$$

For an infinite system, where continuum excitation spectra are involved, taking the average value of the particle-hole matrix element $\bar{F}_{nm}$, Eq. (63) can be approximated, at small $|\varepsilon|$ values, by

$$\begin{aligned}
\text{Im } R^0(\varepsilon, T) &= -\pi \bar{F}_{nm}^2 g_0^2 \int_{-\infty}^{+\infty} dx \int_{-\infty}^{+\infty} dy\, n_F(y)(\delta(\varepsilon - x + y) - \delta(\varepsilon + x - y)) \\
&= -\pi \bar{F}_{nm}^2 g_0^2 \int_{-\infty}^{+\infty} dx (n_F(x-\varepsilon) - n_F(x+\varepsilon)) \\
&= -\frac{\pi \bar{F}_{nm}^2 g_0^2}{\beta} \int_{-\infty}^{+\infty} dx \left(\frac{1}{ae^x + 1} - \frac{1}{e^x + 1} \right) \\
&= -\frac{\pi \bar{F}_{nm}^2 g_0^2}{\beta} \int_0^{+\infty} dt \left(\frac{1}{t+1} - \frac{a}{at+1} \right) \\
&= +\frac{\pi \bar{F}_{nm}^2 g_0^2}{\beta} \ln a \\
&= -2\pi \bar{F}_{nm}^2 g_0^2 \varepsilon,
\end{aligned} \tag{64}$$

where g_0 is the level density at the Fermi energy.

APPENDIX B

In this appendix, the single-particle self-energy Σ in a finite temperature many-body system, due to the coupling of a single-particle state i to uncorrelated particle-hole (p-h) (but also particle-particle (p-p) and hole-hole (h-h)) states, via a separable two-body interaction factorized in terms of a product of two single-particle fields $\hat{F}$, is given. The real and imaginary parts of Σ and an estimation of the temperature dependence of the effective mass are then obtained in the case of an infinite system.

In the case of coupling to an uncorrelated p-p, p-h, or h-h state, the single-particle self-energy is given by

$$\begin{aligned}
\Sigma_i(ip_n, T) = k^2 \sum_{nfm} F_{if}^2 F_{nm}^2 \frac{1}{\beta} \sum_{ip_n''} \mathcal{G}^0(f, ip_n + ip_n'') \\
\times \frac{1}{\beta} \sum_{ip_n'} \mathcal{G}^0(n, ip_n') \mathcal{G}^0(m, ip_n' + ip_n'').
\end{aligned} \tag{65}$$

The sum over ip'_n represents the calculation of the "bubble" diagram (see Appendix A, Eq. (59)). Defining $\varepsilon_{nm} = \varepsilon_n - \varepsilon_m$, Eq. (65) reduces to

$$\begin{aligned}\Sigma_i(ip_n, T) &= k^2 \sum_{nfm} F_{if}^2 F_{nm}^2 (n_F(\varepsilon_n) - n_F(\varepsilon_m)) \\ &\quad \times \frac{1}{\beta} \sum_{ip''_n} \frac{1}{ip_n + ip''_n - \varepsilon_f} \frac{1}{ip''_n - \varepsilon_m + \varepsilon_n} \\ &= k^2 \sum_{nfm} F_{if}^2 F_{nm}^2 \frac{(1 + n_B(\varepsilon_{nm}) - n_F(\varepsilon_f))(n_F(\varepsilon_m) - n_F(\varepsilon_n))}{ip_n - \varepsilon_f - \varepsilon_{nm}} \\ &= k^2 \sum_{nfm} F_{if}^2 F_{nm}^2 n_F(\varepsilon_m) \\ &\quad \times \left[\frac{(1 + n_B(\varepsilon_{nm}) - n_F(\varepsilon_f))}{ip_n - \varepsilon_f - \varepsilon_{nm}} - \{\varepsilon_{nm} \to -\varepsilon_{nm}\} \right]. \end{aligned} \tag{66}$$

Performing the substitution $ip_n \to \varepsilon + i\eta$, the retarded self-energy is obtained, corresponding to Eq. (3) in the text.

Equation (6) in the text is solved taking the mean value of the matrix elements ($v = k\bar{F}_{if}\bar{F}_{nm}$) and replacing sums by integrals (via the introduction of the level density g_0). By virtue of the identity

$$n_B(\omega) + n_F(\omega - \varepsilon) = \frac{(1 + a)\, e^{\beta\omega}}{(e^{\beta\omega} - 1)(ae^{\beta\omega} + 1)}, \tag{67}$$

with $a = e^{-\beta\varepsilon}$, then

$$\begin{aligned}\operatorname{Im} \Sigma_i^{ret}(\varepsilon, T) &= 2\pi\bar{v}^2 g_0^3 \int_{-\infty}^{+\infty} d\omega\, \omega (n_B(\omega) + n_F(\omega - \varepsilon)) \\ &= 2\pi\bar{v}^2 g_0^3 (1 + a) \int_{-\infty}^{+\infty} d\omega \frac{\omega e^{\beta\omega}}{(e^{\beta\omega} - 1)(ae^{\beta\omega} + 1)} \\ &= \frac{2\pi\bar{v}^2 g_0^3 (1 + a)}{a\beta^2} \int_0^{+\infty} dt \frac{\ln t}{(t - 1)(t + a^{-1})}, \end{aligned} \tag{68}$$

where the substitution $t = e^{\beta\omega}$ has been performed. The integral in Eq. (68) is given in Ref. [23, p. 533] and gives

$$\int_0^{+\infty} dt \frac{\ln t}{(t - 1)(t + a^{-1})} = \frac{\pi^2 + (\ln a^{-1})^2}{2(1 + a^{-1})}. \tag{69}$$

In terms of $T = 1/\beta$, Eq. (68) finally gives

$$\operatorname{Im} \Sigma_i^{ret}(\varepsilon, T) = \pi\bar{v}^2 g_0^3 [(\pi T)^2 + \varepsilon^2]. \tag{70}$$

To obtain $\mathrm{Re}\,\Sigma_i^{ret}(\varepsilon, T)$, let us make use of Eq. (8), which gives

$$\mathrm{Re}\,\Sigma_i^{ret}(\varepsilon, T) \approx \bar{v}^2 g_0^3 \mathscr{P} \int_{-c}^{+c} dx\, \frac{\tau^2 + x^2}{\varepsilon - x} + F(x) \tag{71}$$

where $\tau = \pi T$. Thus

$$\begin{aligned}\mathrm{Re}\,\Sigma_i^{ret}(\varepsilon, T) &\approx -\bar{v}^2 g_0^3 \left[\int_{-c-\omega}^{+c-\omega} dx(x + 2\omega) + (\omega^2 + \tau^2)\, \mathscr{P} \int_{-c-\omega}^{+c-\omega} \frac{dx}{x} \right] + F(x) \\ &= -\bar{v}^2 g_0^3 \left[2\omega c + (\omega^2 + \tau^2) \ln \frac{c - \omega}{c + \omega} \right] + F(x) \end{aligned} \tag{72}$$

which is Eq. (11) in the text. Finally, the effective mass enhancement, given in Eq. (12), is obtained by the derivative at the Fermi energy of Eq. (72),

$$\begin{aligned} -\left(\frac{d\,\mathrm{Re}\,\Sigma^{ret}(\varepsilon, T)}{d\varepsilon} \right)_{\varepsilon \sim 0} &\sim \bar{v}^2 g_0^3 \left[2c + \tau^2 \frac{\partial}{\partial \varepsilon} \left(\ln \frac{c - \varepsilon}{c + \varepsilon} \right)_{\varepsilon = 0} \right] \\ &= \bar{v}^2 g_0^3 \left[2c - \frac{2\tau^2}{c} \right] \\ &= 2\bar{v}^2 c g_0^3 \left[1 - \left(\frac{\pi T}{c} \right)^2 \right]. \end{aligned} \tag{73}$$

APPENDIX C

In this Appendix, the single-particle self-energy Σ in the finite temperature slab model, due to the coupling of a single-particle state i to surface vibrations, is obtained.

The imaginary part of $\mathrm{Im}\,\Sigma_i^{ret}$, in the case of the particle-vibration coupling, is given by Eq. (32), where the lower integration limit is K_0 instead of 0 and where the K-integration is given in Eq. (36). Therefore, using the oddness of the arc tangent function and some usual property of the occupation factors, one finds

$$\begin{aligned} \mathrm{Im}\,\Sigma_i^{ret}(\varepsilon, T) &= \frac{\bar{F}_{if}^2}{4\pi\sigma}\, g_0 \int_{-\infty}^{+\infty} d\omega (n_B(\omega) + n_F(\omega - \varepsilon))\, \mathrm{arc\,tan} \frac{a\omega}{\sigma K^2} \\ &= \frac{\bar{F}_{if}^2}{4\pi\sigma}\, g_0 \int_0^{+\infty} d\omega (2n_B(\omega) + n_F(\omega + \varepsilon) + n_F(\omega - \varepsilon)) \\ &\quad \times \mathrm{arc\,tan} \frac{a\omega}{\sigma K^2}. \end{aligned} \tag{74}$$

Then we split the integration domain in two regions, $\omega < \omega_0$ and $\omega > \omega_0$, where we use the linear and the asymptotic (constant) approximations of the arc tangent. Then, Eq. (74) becomes

$$\begin{aligned}&\mathrm{Im}\,\Sigma_i^{ret}(\varepsilon, T)\\&\quad=\frac{\bar{F}_{if}^2}{8\sigma}\,g_0\left[\int_{\omega_0}^{+\infty} d\omega(n_B(\omega)+n_F(\omega-\varepsilon))+\int_0^{+\omega_0} d\omega\,\frac{\omega}{\omega_0}\left(\frac{2T}{\omega}+1\right)\right],\end{aligned}\tag{75}$$

where the second integral is obtained retaining only the low-frequency dominating terms in the occupation factors. The second integral gives an energy-independent term,

$$\begin{aligned}\frac{\bar{F}_{if}^2}{8\sigma}\,g_0\int_0^{+\omega_0} d\omega\,\frac{\omega}{\omega_0}\left(\frac{2T}{\omega}+1\right)&=\frac{\bar{F}_{if}^2}{8\sigma}\,g_0\left(2T+\frac{\omega_0}{2}\right)\\&\approx\frac{\bar{F}_{if}^2}{4\sigma}\,g_0\,T,\end{aligned}\tag{76}$$

where the contribution of the constant, temperature-independent term ω_0 can be neglected (choosing $K_0 = 0.1\ \mathrm{fm}^{-1}$, then $\omega_0/2 = 0.05$ MeV). The first integral contribution can also be split in two terms. Unless we have the constant factor $k_i^2/(8\sigma)$, we have the energy-independent term,

$$\mathscr{I}_1=\int_{\omega_0}^{+\infty} d\omega\,n_B(\omega)=\frac{1}{\beta}\ln(1+n_B(\omega_0)),\tag{77}$$

while all the energy dependence is contained in the second one which gives, defining $a = e^{\beta\varepsilon}$,

$$\begin{aligned}\mathscr{I}_2&=\int_{\omega_0}^{+\infty} d\omega(n_F(\omega+\varepsilon)+n_F(\omega-\varepsilon))\\&=\int_{\omega_0}^{+\infty} d\omega\,\frac{1}{(1+ae^{\beta\omega})}+\int_{\omega_0}^{+\infty} d\omega\,\frac{1}{(1+a^{-1}e^{\beta\omega})}\\&=\frac{1}{a\beta}\int_{e^{\beta\omega_0}}^{+\infty}\frac{dt}{t}\frac{1}{t+a^{-1}}+\frac{a}{\beta}\int_{e^{\beta\omega_0}}^{+\infty}\frac{dt}{t}\frac{1}{t+a}\\&=\frac{1}{\beta}\left[-2\omega_0\beta+\ln|e^{\beta\omega_0}+a|+\ln|e^{\beta\omega_0}+a^{-1}|\right]\\&=-\frac{1}{\beta}\ln n_F(\varepsilon-\omega_0)(1-n_F(\varepsilon+\omega_0)).\end{aligned}\tag{78}$$

Finally,

$$\begin{aligned}\mathrm{Im}\,\Sigma_i^{ret}(\varepsilon, T) &= \frac{\bar{F}_{if}^2}{8\sigma}\, g_0(2\mathscr{I}_1 + \mathscr{I}_2) + \frac{\bar{F}_{if}^2}{4\sigma}\, g_0 T \\ &= -\frac{\bar{F}_{if}^2}{8\sigma}\, g_0\, T[\ln(n_F(\varepsilon)(1-n_F(\varepsilon))) - 2(1+\ln(1+n_B(\omega_0)))]. \end{aligned} \tag{79}$$

For the evaluation of the real part of the single-particle self-energy, we follow the same scheme adopted in the previous case, but using the parametrization given in Eq. (46). The principal value integral to be solved is

$$\mathscr{P}\int_{-c}^{c} d\omega\, \frac{\sqrt{\omega^2 + (\alpha T)^2}}{\varepsilon - \omega} = \mathscr{P}\int_{\varepsilon - c}^{\varepsilon + c} dx\, \frac{\sqrt{R(x)}}{x}, \tag{80}$$

where $\alpha = 2\ln 2$ and

$$R(x) = (\alpha T)^2 + \varepsilon^2 - 2\varepsilon x + x^2. \tag{81}$$

The solution of this integral can be found in Ref. [23, p. 84] and gives the expression corresponding to Eq. (47).

ACKNOWLEDGMENTS

N. G. thanks both the Niels Bohr Institute and ECT* (Trento) for hospitality and financial support. Suggestions of G. F. Bertsch have stimulated us in carrying out the analysis presented in this paper. Discussions with H. Esbensen, E. Montaldi, A. Jackson, A. Polleri, and T. Doessing are gratefully acknowledged.

REFERENCES

1. G. F. Bertsch and R. A. Broglia, "Oscillations in Finite Quantum Systems," Cambridge Univ. Press, Cambridge, UK, 1994.
2. P. F. Bortignon, A. Bracco, and R. A. Broglia, "Giant Resonances, Nuclear Structure at Finite Temperature," Harwood Academic, New York, 1998.
3. G. D. Mahan, "Many-Particle Physics," Plenum, New York, 1988.
4. B. R. Mottelson, *in* "Proc. Int. School of Phys., Enrico Fermi, Course LXIX" (A. Bohr and R. A. Broglia, Eds.), p. 31, North-Holland, Amsterdam, 1977; D. Pines and P. Nozières, "The Theory of Quantum Liquids," Vol. I, Addison–Wesley, Reading, MA, 1966.
5. A. L. Fetter and J. D. Walecka, "Quantum Theory of Many-Particle Systems," McGraw–Hill, New York, 1971.
6. P. Donati *et al.*, *Phys. Rev. Lett.* **72** (1994), 2835.

7. P. Donati *et al.*, *Z. Phys. A* **354** (1996), 249.
8. P. Donati *et al.*, *Phys. Lett. B* **383** (1996), 15.
9. H. Esbensen and G. F. Bertsch, *Ann. Phys.* **157** (1984), 255.
10. R. A. Broglia, O. Hansen, and C. Riedel, *Adv. Nucl. Phys.* **6** (1973), 287.
11. C. Mahaux *et al.*, *Phys. Rep.* **120** (1985), 1.
12. A. Bohr and B. R. Mottelson, "Nuclear Structure," Vol. I, Benjamin, New York, 1969.
13. P. Morél and P. Nozières, *Phys. Rev.* **126** (1962), 1909.
14. P. F. Bortignon and C. H. Dasso, *Phys. Lett. B* **189** (1987), 381.
15. A. Bohr and B. R. Mottelson, "Nuclear Structure," Vol. II, Benjamin, New York, 1975.
16. H. Sagawa and G. F. Bertsch, *Phys. Lett. B* **146** (1984), 138.
17. H. Esbensen and G. F. Bertsch, *Phys. Lett. B* **161** (1985), 248.
18. H. Esbensen and G. F. Bertsch, *Phys. Rev. Lett.* **52** (1984), 2257.
19. G. F. Bertsch, P. F. Bortignon, and R. A. Broglia, *Rev. Mod. Phys.* **55** (1983), 287.
20. P. F. Bortignon *et al.*, *Nucl. Phys. A* **460** (1986), 149.
21. B. Lauritzen *et al.*, *Phys. Rev. Lett.* **74** (1995), 5190.
22. C. Mahaux and R. Sartor, *Adv. Nucl. Phys.* **20** (1991), 1.
23. I. S. Gradshteyn and I. M. Ryzhik, "Table of Integrals, Series and Products," Academic Press, San Diego, 1992.